JOURNAL OF AIRCRAFT
Vol. 34, No. 3, May–June 1997

Critical-State Transients for a Rolling 65-Degree Delta Wing

Deborah S. Grismer* and Jerry E. Jenkins†
U.S. Air Force Wright Laboratory, Wright–Patterson Air Force Base, Ohio 45433-7521

Force and moment experiments were conducted for a 65-deg delta wing undergoing ramp-and-hold and harmonic rolling motions. This extensive set of experiments isolated critical-state responses. Motions between critical states and motions crossing critical states were included. Roll-angle amplitude and the roll rate were varied. The total angle of attack and Mach number were held constant at 30 deg and 0.3, respectively. The amount of time required for the rolling moment coefficient to reach its steady-state value after the end of a ramp was quantified for numerous ramp motions. This relaxation time was a significantly large value for many of the motions, especially when the 5-deg critical state was crossed. Motion history effects were determined for motions that crossed critical states. The effect of roll rate on critical-state transients proved to be insignificant.

Nomenclature

b = trailing-edge wing span
C_l = rolling moment/qSb
$C_{l_{dyn}}$ = $C_l - C_{l_{static}}$
c = root chord
$\bar{c}$ = mean aerodynamic chord
k = reduced frequency, $\omega b/2U_\infty$
q = freestream dynamic pressure
S = model planform area
t = time
t^* = nondimensional time, $2U_\infty t/b$
U_∞ = freestream velocity
σ = total angle of attack, body-axis inclination with respect to U_∞
ϕ = body-axis roll angle $\cong \phi_1$
$\dot{\phi}$ = first derivative of ϕ with respect to time
$\ddot{\phi}$ = second derivative of ϕ with respect to time
ϕ_{ND} = nondimensional roll rate, $\dot{\phi}(b/2U_\infty)$
ϕ_1 = shaft rotation angle at the base of the sting
ϕ_2 = shaft rotation angle at the center of the force balance
ω = circular frequency, rad/s

Introduction

AN expansion of the flight envelope has been and remains a very important goal for designers of high-performance air vehicles. Such high-performance aircraft are required to fly faster and at higher angles of attack. Because of these demands they often employ highly swept wing surfaces. When flying at higher angles of attack, controllability has become a large problem for these aircraft. Intense changes in the flowfield are encountered that result in dramatic nonlinearities in an aircraft's aerodynamic behavior. Under these conditions the aerodynamics are time- and motion-history-dependent; therefore, conventional quasisteady modeling techniques are not adequate.

This paper will discuss some implications of experimental force and moment results for a 65-deg delta wing driven through roll maneuvers. This delta wing has been the focus of an in-depth study over the past several years.[1–11] Previous analyses of the delta wing have shown severe nonlinear aerodynamic behavior and the aerodynamics have been shown to be dependent on the precise motion history. As with other highly swept planforms, vortex breakdown was found to be a large contributor to the aerodynamic behavior of the 65-deg delta wing. The axial progression of breakdown because of a time-dependent variation in wing orientation was found to be quite slow.

The dynamic force and moment responses possessed large time lags. Two possible causes for these time lags are 1) finite response times caused primarily by the response of vortex breakdown and 2) transients resulting from one or more critical-state encounters. A critical state exists when a discontinuity in a static force or moment curve (or its derivative) occurs and its crossing causes a discrete change in the equilibrium response. Thus, time lags can result without encountering a critical state, but if a critical state is encountered, there is an additional amount of time that is required for the transition from one flow state to another. The time scales for these critical-state transients had not been established. For modeling purposes and possible simplifications, it would be very useful to know if the effects from one or more critical-state encounters can be neglected.

The force and moment experiments of this study were designed to isolate the effects induced by critical-state encounters. Measurements were obtained for ramp-and-hold motions and harmonic motions in roll. Comprehensive static and dynamic force and moment measurements were obtained. An examination of these results will be the focus of this paper, with the goal being to increase the knowledge of how to better model the transients induced from critical-state encounters.

Discussion

Experimental Equipment

The model used for the experiments was a 65-deg delta wing with sharp leading and trailing edges. A schematic of the model is shown in Fig. 1. Both the leading and trailing edges were symmetrically beveled with an included angle normal to the leading edge of 20 deg. The wing was constructed with a multilayer graphite composite skin and a foam core, and the fuselage was constructed purely of graphite composite. The wing thickness-to-root-chord ratio is 1.53%.

The delta wing was mounted in the Subsonic Aerodynamic Research Laboratory (SARL) 7 ft × 10 ft (2.1 m × 3.0 m)

Presented as Paper 96-2432 at the AIAA 14th Applied Aerodynamics Conference, New Orleans, LA, June 17–20, 1996; received Aug. 24, 1996; revision received Feb. 12, 1997; accepted for publication Feb. 17, 1997.

*Captain, U.S. Air Force, Flight Control Division, Flight Dynamics Directorate, WL/FIGC, Building 146, 2210 Eighth Street, Suite 11. Member AIAA.

†Aerospace Engineer, Flight Control Division, Flight Dynamics Directorate, WL/FIGC, Building 146, 2210 Eighth Street, Suite 11. Senior Member AIAA.

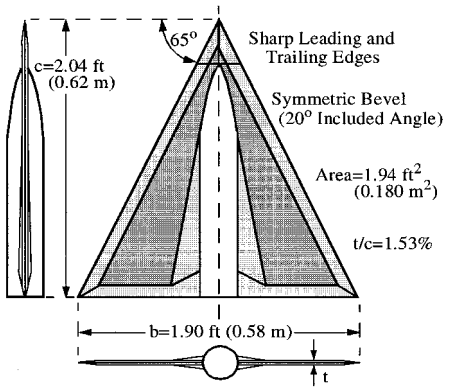

Fig. 1 Delta wing model.

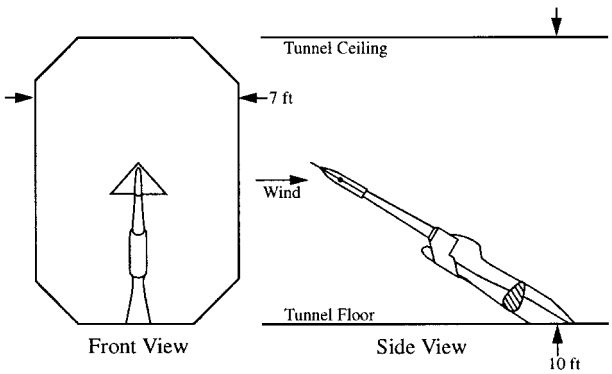

Fig. 2 Roll rig apparatus in SARL wind tunnel.

wind tunnel via a roll rig. The wing was mounted on a five-component strain gauge balance that was supported, by a drive shaft, through a hollow sting. The dynamic roll rig, installed in the SARL tunnel, is shown in Fig. 2. The apparatus, developed by the Canadian National Aeronautical Establishment (NAE), was designed for large-amplitude and high-rate motions. A more detailed description of both the model and roll rig design can be found in Ref. 12.

Data Acquisition and Reduction

The data presented here were obtained from a series of experiments designed and conducted both by personnel from Wright Laboratory and members of the Canadian Institute for Aerospace Research (IAR) in 1994. The delta wing was driven through both ramp-and-hold maneuvers and harmonic oscillations in roll. During these experiments, digitally sampled time histories of both the model motion and five-component force and moment responses were obtained.

For all roll motions presented here the total angle of attack σ was fixed at 30 deg and the Mach number was 0.3. Data were acquired with a constant sampling interval for a given motion and for several (usually 20) cycles of the motion. Five-component force and moment data were ensemble-averaged to yield 1024 data points for one cycle. The five components produced were normal force, pitching moment, side force, yawing moment, and rolling moment. The shaft rotation angle at the base of the sting was also measured throughout the same sampling time. For each motion data were acquired both with the tunnel operating at the desired testing speed and with the wind off.

Ramp Motions

The constant ramp roll rate was varied from 0.25 rad/s (14 deg/s) through 7 rad/s (400 deg/s) for the various ramp motions. A ramp-up cycle consists of a hold at ϕ_{min}, the ramp-up, a 0.5-s hold at ϕ_{max}, and a return to ϕ_{min}. The data, however, were acquired only for a small amount of time before the ramp up starts, through the ramp up, and for the 0.5-s hold at ϕ_{max} after the end of the ramp. The part of the cycle spent returning to ϕ_{min} and an amount of time at ϕ_{min} before starting the next cycle are not included in the data acquisition sampling period. Data were acquired over a sufficient number of cycles so that the ensemble-averaged data did not change with the acquisition of data over an additional cycle.

The first step taken in the data reduction process was to convert the raw output voltages from the force balance to non-dimensional force and moment coefficients, based on the model geometry. The remaining part of the data reduction was much more involved. For many applications, a simple subtraction of the wind-off tare data from the wind-on data would be an adequate method of removing the inertial effects. However, for the ramp motions at which high angular accelerations were commanded at the beginning and end of the ramp, it was determined that such a subtraction was not appropriate.

For a given ramp-and-hold motion, the difference in the roll angle between the wind-on and wind-off data was very small. Slight differences between the measured and commanded roll angles, however, resulted in severely different accelerations commanded by the servo-system. Because of this, significant oscillations were present in both the wind-on and wind-off rolling moment coefficients, particularly following the commanded accelerations. The oscillations between the wind-on and wind-off runs were not always in-phase because the small roll-angle errors are influenced by the airloads acting on the model. Therefore, a subtraction of the two rolling-moment time histories often increased the amplitude of the oscillations.

The inertial effects were determined by an alternate method and they were subtracted from the wind-on force and moment coefficients, yielding a more accurate result, with significantly smaller oscillations. Knowing the roll angle, the rolling moment contribution caused just by the inertia can be calculated and subtracted from the wind-on rolling moment resulting from both the inertial and aerodynamic effects.

To determine the inertial effects the roll motion history $\phi_1(t)$ from the tare runs was used to calculate $\ddot{\phi}_1(t)$. $\ddot{\phi}_1(t)$ was calculated by taking a second-order central difference in time. The initial and final values of $\ddot{\phi}_1(t)$ were calculated using a second-order one-sided difference. Because of the noise produced from differentiating twice, frequencies in the roll acceleration time histories above 100 Hz were numerically filtered out. Knowing $\ddot{\phi}_1(t)$ and $C_l(t)$ for a tare run, an estimate of the inertia I could be determined assuming a simple one-degree-of-freedom system in roll where

$$C_l(t) = (I/qSb)\ddot{\phi}_1(t) + K \tag{1}$$

K is the value of C_l before and after the ramp when $\ddot{\phi}_1(t) = 0$. This value was near zero, but is included to account for any small biases in the signal. Using a least-squares linear curve fit, values of both I and K were calculated, since q from the wind-on tests S and b are all known. Also, the correlation coefficient could be calculated to assess the validity of the linear correlation assumption. Correlation coefficients from 0.60 to 0.85 were obtained. Plots of C_l vs $\ddot{\phi}_1$ showed noticeable loops around the linear curve fit. Since the rotation angle was sensed at the end of the actuator shaft, it was desired to try to determine the shaft rotation angle at the same location where the rolling moment was measured, at the balance center. It was thought that a difference in the rotation angle between the base of the shaft and the balance center, because of torsional deflections of the drive shaft, might be the cause of the observed loops.

To determine the shaft rotation angle at the balance center ϕ_2 the entire shaft from its base to the center of the balance was modeled as a cylinder of uniform torsional stiffness. This system was modeled as a second-order system in terms of the difference in shaft rotation angle $\Delta\phi$, where $\Delta\phi = \phi_2 - \phi_1$.

Therefore, the system was described by the following equation:

$$\Delta\ddot{\phi}(t) + 2\zeta\omega_n\Delta\dot{\phi}(t) + \omega_n^2\Delta\phi(t) = 0 \qquad (2)$$

ζ and ω_n are the damping ratio and natural frequency of the drive shaft torsional degree of freedom, respectively. $\Delta\phi(t)$ was calculated using the indicial form of the Duhamel integral:

$$\Delta\phi(t) = \phi_2(t) - \phi_1(t) = A(t)\phi_1(0) + \int_0^t A(t-\tau)\dot{\phi}(\tau)\,d\tau \qquad (3)$$

where $A(t) = -e^{nt}[\cos\omega t + (n/\omega)\sin\omega t]$ with $n = -\zeta\omega_n$ and $\omega = \omega_n\sqrt{1-\zeta^2}$. Since $\phi_1(t)$ was known, $\phi_2(t)$ was then determined. $\phi_1(t)$ was found to be essentially identical to $\phi_2(t)$.

Fixed values of ζ and ω_n were found by trying to minimize the difference between the measured $C_l(t)$ and the $C_l(t)$ calculated using $\ddot{\phi}_2(t)$ in Eq. (1). Previous work[11] had shown, however, that the damping force was not proportional to $\dot{\phi}$, but rather it was essentially a constant force opposing the direction of motion. Therefore, ζ was set to be inversely related to $|\dot{\phi}_1|$ to provide a constant damping force. This provided a good match between the measured and calculated values of $C_l(t)$ as desired.

Using the values of I/qSb and K determined by including the tare values of $\ddot{\phi}_2(t)$ in Eq. (1), the necessary information was found to subtract the inertial effects from the wind-on rolling moment data. For ramp motions, the values of $C_l(t)$ discussed in the remainder of this paper were calculated by taking the wind-on measured values of $C_l(t)$ and subtracting $C_l(t)$ calculated from Eq. (1), using the wind-on measured values for $\phi_1(t)$.

Harmonic Motions

The frequency was varied from 1.1 through 11 Hz for the harmonic motions. For these motions one sampling cycle is one complete harmonic oscillation. In these cases, force and moment data were obtained by subtracting the wind-off data from the wind-on data. Obvious oscillations were present in the resulting force and moment time histories. To better smooth the data, a fast Fourier transform was performed and a limited number of harmonics were kept. The number of harmonics retained varied with forcing frequency as shown in Table 1. Determining the number of harmonics to retain was established by choosing a number small enough to provide sufficient smoothing while retaining the overall shape of the time histories.

Observations

Previous findings[1] revealed the existence of a critical state for this delta wing at approximately $\phi = 5$ deg. This can be seen in the static rolling moment coefficient vs ϕ, shown in Fig. 3. In the region of $\phi = 5$ deg a definite discontinuity in the rolling moment coefficient is observed. A discontinuity in the pitching moment coefficient was also observed around this angle. These discontinuities indicate the existence of a subcritical bifurcation. Critical states around 8 and 11.3 deg were also proposed in previous work. The 8-deg critical state is likely to be a Hopf bifurcation because of the large rms fluctuations.[2] The increase in scatter for ~ 8 deg $< \phi < \sim 12$ deg, shown in Fig. 3, indicates that time-averaging failed to average out low-frequency fluctuations. The 11.3-deg critical state appears to be a supercritical bifurcation. Also, the unsteadiness in C_l is greatly reduced for $\phi > \sim 12$ deg.

Table 1 Number of harmonics retained for harmonic motions of varying forcing frequency

Forcing frequency, Hz	Reduced frequency	Number of harmonics kept	Resulting cutoff frequency, Hz
1.1	0.010	8	8.8
2.2	0.021	8	17.6
3.3	0.031	7	23.1
4.4	0.042	6	26.4
5.5	0.052	5	27.5
7.7	0.073	4	30.8
8.8	0.084	4	35.2
11	0.105	3	33.0

Ramp Motions

The experiments were designed to isolate the effects of critical-state encounters from viscous time lags caused primarily by the slow response of vortex breakdown position. Four different ramp motions are shown in Fig. 4. These ramp motions either stay below the critical state around $\phi = 5$ deg, cross the critical state, or stay above the critical state.

Figure 5 illustrates $C_l(t)$ for a ramp motion in roll from 7 to 4 deg at -1 rad/s as compared to the quasisteady $C_l(t)$ over this range in roll angle. This figure reveals an obvious difference between the measured and quasisteady response. Also, it is interesting that at ramp onset the dynamic response is increasing, while the reverse is true of the quasisteady behavior. Note that $C_l(t)$ does not approach the quasisteady value until long after the ramp has ended. The amount of time required for the rolling moment coefficient after the end of a ramp ($\dot{\phi} \approx 0$) to reach its quasisteady value was quantified for many motions.

It was desired to isolate the transient effects resulting from the presence of the leading-edge vortices. Previous findings[13]

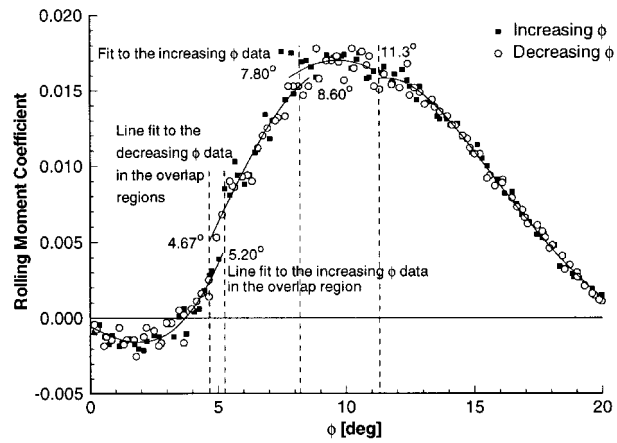

Fig. 3 Time-averaged static C_l for both increasing and decreasing ϕ.[1]

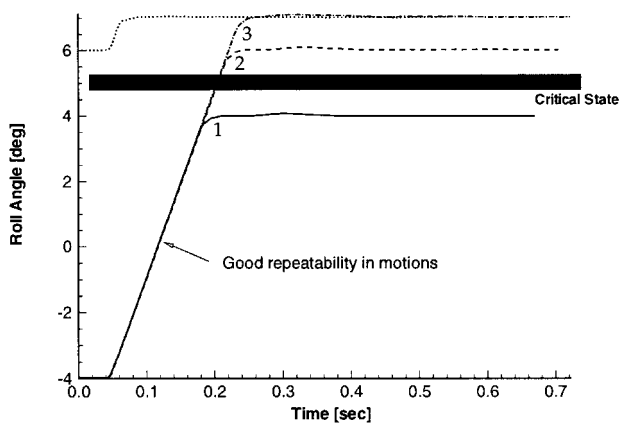

Fig. 4 Sample (1 rad/s) ramp motions about the 5-deg critical state.

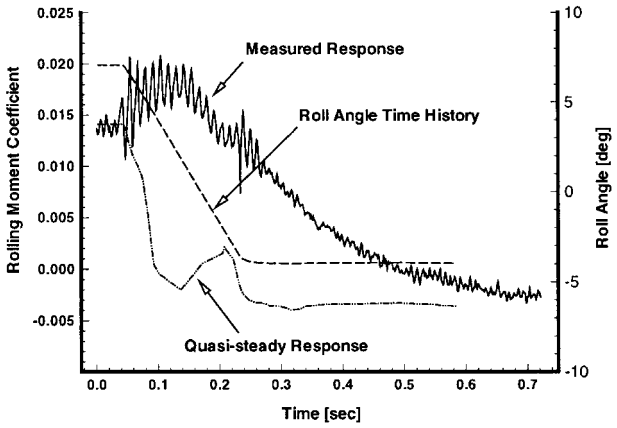

Fig. 5 Static and dynamic C_l for a (−1 rad/s) ramp through the 5-deg critical state.

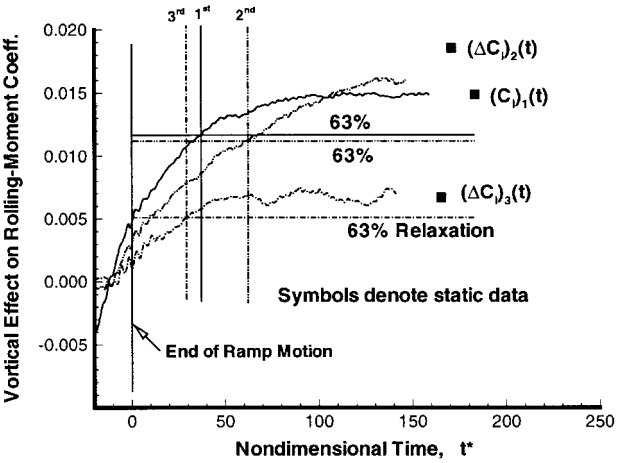

Fig. 6 Determination of relaxation times for ramp motions through the 5-deg critical state ($\dot{\phi}_{ND} = 0.003$).

revealed that the vortical component of the rolling moment had a net destabilizing effect for roll-angle variations. The presence of vortex breakdown and its relatively slow response is considered to be the dominant cause of time lags observed for dynamic maneuvers (not counting critical-state effects). The potential flow component of the rolling moment reacts at the freestream convection speed, which for these rates can be considered virtually instantaneous. Therefore, the potential flow part of the rolling moment coefficient was subtracted from the total rolling moment coefficient. The potential contribution was calculated using QUADPAN, a panel code developed by Lockheed–California Company.[14]

Figure 6 shows the vortical contribution to the rolling moment coefficient, the total rolling moment minus the potential contribution. This figure illustrates how relaxation times were calculated. The first, second, and third rolling moment coefficients correspond to ramp motions from −4 deg to 4, 6, and 7 deg, respectively, each for a roll rate of 1 rad/s, as shown in Fig. 4. For each of these three ramp motions the vortical rolling moment responses were time-shifted so that a nondimensional time of 0.0 corresponded to the end of each of the ramp motions. Also, the second vortical rolling moment coefficient $(\Delta C_l)_2$, shown in Fig. 6, has the response of the first motion subtracted. Likewise, the third response had the response from the second motion subtracted.

The relaxation times that were quantified, as shown in Fig. 6, were actually the time after the end of the ramp until the rolling moment coefficient reached 63% of its value at the end of the ramp-and-hold. This value of 63% was chosen because, for an exponential decaying function $C_l(t)$, where $\Delta C_l(t) = C_{l_{static}}[1 - e^{-(t/a)}]$, with $C_l(t \to \infty) = C_{l_{static}}$, and $C_l(t = a) = 0.632C_{l_{static}}$. a must have the same units as t and it is called the time constant. The relaxation times, according to this definition, are indicated by vertical lines. It should be noted, as evidenced by Fig. 6, that these calculations of the relaxation times are conservative because they did not take the time-averaged static values (denoted by solid symbols) to be the necessary equilibrium value. The second ramp motion, which crosses the critical state, illustrates that even at the end of the sampling period the vortical rolling moment contribution has not yet reached the static value.

These (63%) relaxation times were quantified for several ramp motions with positive and negative roll rates about various critical states. The nondimensional relaxation times $t^*_{63\%}$, as well as the $\Delta C_{l_{max}}$ (from the end of the ramp to the assumed steady-state value) are included in Table 2.

Table 2 reveals the relaxation time constant about the 5-deg critical state ($t^*_{63\%} \approx 70$) to be quite large. The 8-deg critical state yielded a lower value ($t^*_{63\%} \approx 50$). Calculations of the relaxation time constants for the 11.3-deg critical state, although not included in the table, found $t^*_{63\%} \approx 10$. The $\Delta C_{l_{max}}$ values used to calculate the relaxation time constants for the 11.3-deg critical state, however, were very small. Therefore, these relaxation time constants were less meaningful. This might be expected from Fig. 3, which shows that for roll-angle variations around 11.3 deg, the difference in the static rolling-moment coefficient is small.

The relaxation time constants calculated for ramp motions that did not involve crossing a critical state yielded values of $t^*_{63\%} \approx 30$. For these motions, where vortex breakdown existed over the wing, the time constant reflects the relaxation time resulting from the response of vortex breakdown.

The range of ramp motions examined allowed history effects across critical states to be assessed. As shown in Fig. 4, ramp motions were conducted for ϕ between −4 and 6 deg, between −4 and 7 deg, and between 6 and 7 deg. The rolling-moment data obtained for the ramp from 6 to 7 deg were compared to the rolling moment data for the ramp from −4 to 7 deg with the rolling-moment data for the ramp from −4 to 6 deg subtracted. The result of this subtraction is denoted Δ = 6 to 7 deg. This comparison is shown in Fig. 7a. Note again that the potential flow contribution to the rolling moment was subtracted, leaving just the vortical contribution. This plot reveals no significant history effects on the rolling moment coefficient in the ϕ range from 6 to 7 deg after crossing the 5-deg critical state. Table 2 also illustrates that the time constants ($t^*_{63\%} \approx 30$) determined for Δ = 6 to 7 deg were approximately equal to the time constant determined for a direct ramp motion from 6 to 7 deg.

The same type of procedure was used to examine the history effect on the subsequent response after passing through the 8-deg critical state. Figure 7b illustrates the comparison between the vortical rolling moment coefficient for a ramp from 9 to 10 deg with a ramp from 6 to 10 deg, subtracting the history of the ramp from 6 to 9 deg. This comparison illustrates a noticeable difference between the two results. Therefore, including the flow history from 6 to 9 deg, which crosses the 8-deg critical state, produced a distinctly different transient response over the 9- to 10-deg range. The causes for and conditions under which critical-state history effects become important are not yet understood. This will be a subject of future investigations.

The effect of roll rate on the critical-state transients was investigated using the data obtained with different roll rates over the same roll-angle range. Figure 8, which contains the vortical contribution to the rolling moment coefficient for three different roll rates, reveals that the roll rate has no significant effect on the transients for the 5-deg critical state. Again, Table 2 illustrates that the time constants for each roll rate were all approximately $t^*_{63\%} \approx 70$.

Table 2 Relaxation times to 63% of steady-state values for various ramp motions

Critical state, deg	Rate rad/s, ND	Up/down	Precritical state $t^*_{63\%}$	Precritical state $\Delta C_{l_{max}}$	Crossing critical state $t^*_{63\%}$	Crossing critical state $\Delta C_{l_{max}}$	Postcritical state $t^*_{63\%}$	Postcritical state $\Delta C_{l_{max}}$
5			−4 to 4 deg		−4 to 6 deg Δ = 4 to 6 deg[a]		−4 to 7 deg Δ = 6 to 7 deg	
	1 (0.003)	Up	36	0.010	62	0.014	30	0.006
	4 (0.012)	Up	33	0.014	68	0.014	40	0.007
	7 (0.020)	Up	33	0.014	73	0.006	47	0.007
			7 to 6 deg		7 to 4 deg Δ = 6 to 4 deg		7 to −4 deg Δ = 4 to −4 deg	
	1 (0.003)	Down	24	−0.006	61	−0.014	78	−0.010
8			6 to 7 deg		6 to 9 deg Δ = 7 to 9 deg		6 to 10 deg Δ = 9 to 10 deg	
	1 (0.003)	Up	33	0.006	42	0.009	5	0.004
			10 to 9 deg		10 to 7 deg Δ = 9 to 7 deg		10 to 6 deg Δ = 7 to 6 deg	
	1 (0.003)	Down	14	−0.002	53	−0.008	34	−0.005

[a]Δ = 4 to 6 deg denotes moment response for ϕ from −4 to 4 deg was subtracted from moment response for ϕ from −4 to 6 deg.

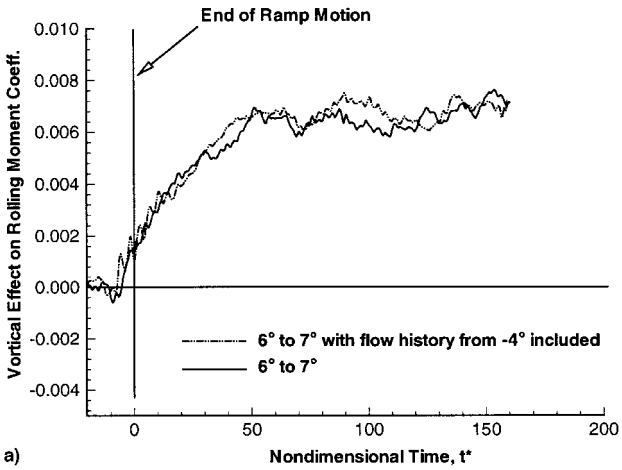

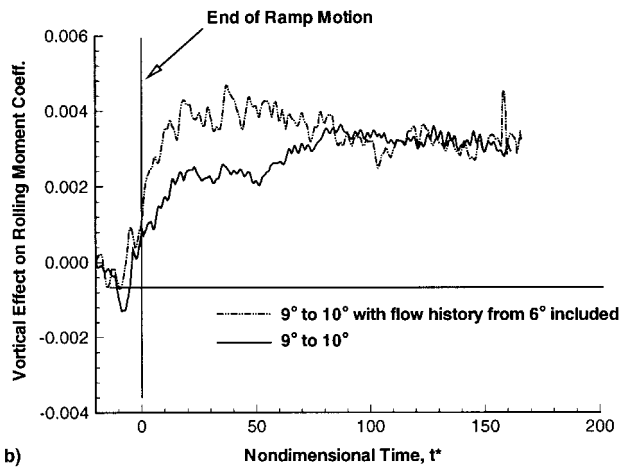

Fig. 7 Response of the vortical contribution to C_l with and without the prior motion history through the a) 5- and b) 8-deg critical state included ($\dot{\phi}_{ND}$ = 0.003).

Harmonic Motions

The rolling-moment responses for numerous harmonic roll oscillations were obtained. Figure 9 contains rolling-moment-coefficient responses for 5-deg amplitude harmonic oscillations in roll. These oscillations, which vary in frequency from 1.1 to 11 Hz ($0.010 \leq k \leq 0.105$), are centered about ϕ = 3 deg. The solid symbols in Fig. 9 show the static results and the dashed curve shows the static potential flow contribution to C_l. These C_l loops run in a counterclockwise sense, therefore,

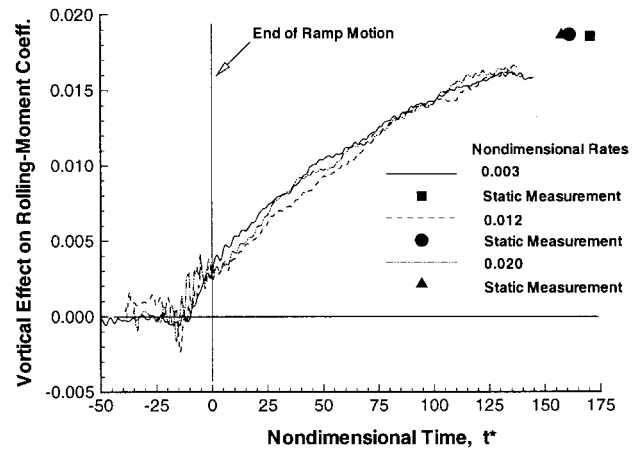

Fig. 8 Roll-rate effect on the transient C_l response through the 5-deg critical state.

at a given ϕ, C_l on the upstroke is less than C_l on the downstroke.

For the oscillation of lowest frequency, k = 0.010, C_l attempts to follow the curvature of the static data. As the frequency is increased, however, the deviation from the static data becomes more apparent. For all but the lowest frequency the rolling moment response no longer even remotely resembles the curvature of the static data. For each oscillation shown in Fig. 9, C_l for ϕ_{min} and ϕ_{max} were obtained. A line (dash-double-dot) is shown connecting these two values for each oscillation. Even at the lowest frequency, C_l values at the roll angle limits ($\dot{\phi} \approx 0$) do not reach their static values. With increasing frequency the slope of the line connecting the roll angle limits moves closer to the slope of the potential flow contribution. It would be expected that for a harmonic oscillation of very large frequency, the flow would respond only to the virtually instantaneously reacting flow component. Furthermore, the amplitude of the rolling-moment response loops decreases as frequency increases. Figure 9 also illustrates that on the upstroke, in the range of the offset angle, ϕ = 3 deg, the value of C_l is virtually independent of roll rate. However, on the downstroke, after crossing the 5-deg critical state, the roll rate has a significant effect on the rolling-moment coefficient.

Using the nonlinear indicial response model (NIR) and the superposition integral (presented in detail in previous papers[15,16]), the classic Taylor-series expansion for the aerodynamic response to a motion input can be derived.[17] When these results are specialized to the case of forced harmonic motion, relationships are established between specific stability derivatives (both linear and nonlinear) and the variation of the aero-

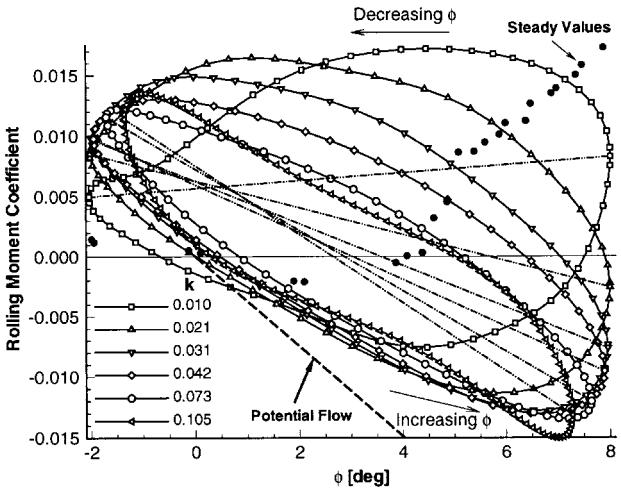

Fig. 9 C_l **response to 5-deg-amplitude harmonic motions centered at** $\phi = 3$ **deg.**

dynamic responses at harmonics of the forcing frequency. That is, for the steady-state response to a harmonic motion input; e.g.,

$$\phi(t) = \phi_0 + \Delta\phi \cos(kt) \tag{4}$$

the rolling moment response can be shown to be of the form

$$C_{l_{dyn}} = C_{l_0} + F_1\cos(kt) + F_2\cos(2kt) + F_3\cos(3kt) + \cdots + G_1\sin(kt) + G_2\sin(2kt) + G_3\sin(3kt) + \cdots \tag{5}$$

where each of the in-phase coefficients F_n is a summation of the contributions $f_{n,j}$ from particular stability parameters that are designated by the subscript j. Therefore,

$$F_n = \sum_{j=1}^{j_{max}} f_{n,j}$$

Similarly, out-of-phase terms G_n also consist of contributions $g_{n,j}$. The individual contributions can be factored into the form

$$\begin{aligned} f_{n,j} &= \bar{f}_{n,j}(\phi_0, \Delta\phi)[a_2k^2 + a_4k^4 + \cdots] \\ g_{n,j} &= \bar{g}_{n,j}(\phi_0, \Delta\phi)k[b_1 + b_3k^2 + b_5k^4 + \cdots] \end{aligned} \tag{6}$$

Note that the frequency effect appears as a power series in k. Also, the coefficients of these terms, (a_i, b_i), correspond to the relevant stability derivative. Furthermore, the higher-order terms (in k) arise from repeated differentiation of the motion parameters.[17] Differentiation of $\sin(nkt)$ gives $nk\cos(nkt)$. That is, the series proceeds in the order $b_1(nk) + a_2(nk)^2 + \cdots$. Thus, if

$$k > 1/(na_2/b_1)$$

the series diverges.

It must also be noted that this analysis is valid under the following conditions:

1) The motion is analytic (which is true for forced oscillation tests).

2) The motion does not cross a critical state.

3) Time constants for the indicial response transients are less than $1/nk$, where nk is the frequency of the affected harmonic.

The convergence properties of the series representation (when applied to harmonic motion) can be used to provide an independent check of indicial response time scales. From ramp-and-hold motion data (see Table 2), indicial response time constants of about 30 are expected in the roll angle range between the critical states at ±5 deg. Thus, for harmonic motions in this range, the series approximation is expected to converge for reduced frequencies below about 0.033. Therefore, harmonic motions (centered about 0-deg roll angle and with amplitudes of 2, 3, and 4 deg) at the two lowest frequencies, $k = 0.02$ and 0.04, were analyzed. A stepwise regression analysis[7] was used to identify the most significant terms in the series expansion. The correlation coefficient for the regression was 0.886, and comparisons between experimental and predicted $C_{l_{dyn}}$ are shown in Figs. 10a and 10b. Although the data trends with frequency and amplitude are well captured by the regression model, the overall agreement may be compromised by the fact that $k = 0.04$ slightly exceeds the expected range of applicability.

Four separate contributions were identified; i.e., $j_{max} = 4$. The results are summarized in Table 3. As shown, the key contributors are the first and fourth parameters, both showing divergence for $k \approx 0.04$. Thus, these results also show that application of the procedure to data taken at $k = 0.04$ is marginal. Moreover, the regression analysis confirms that indicial response time constants, as determined from ramp and hold maneuvers, are correct within approximately 10%. It also suggests

Table 3 Regression results

j	Parameter	Harmonic, n	na_2/b_1	k_{crit}
1	Linear, $\dot{\phi}$	1	28.4	0.035
2	$\phi^2\dot{\phi}$	1	19.5	0.051
3	$\phi\phi\dot{\phi}$	1	16.0	0.063
4	$\phi\dot{\phi}$	2	24.8	0.040

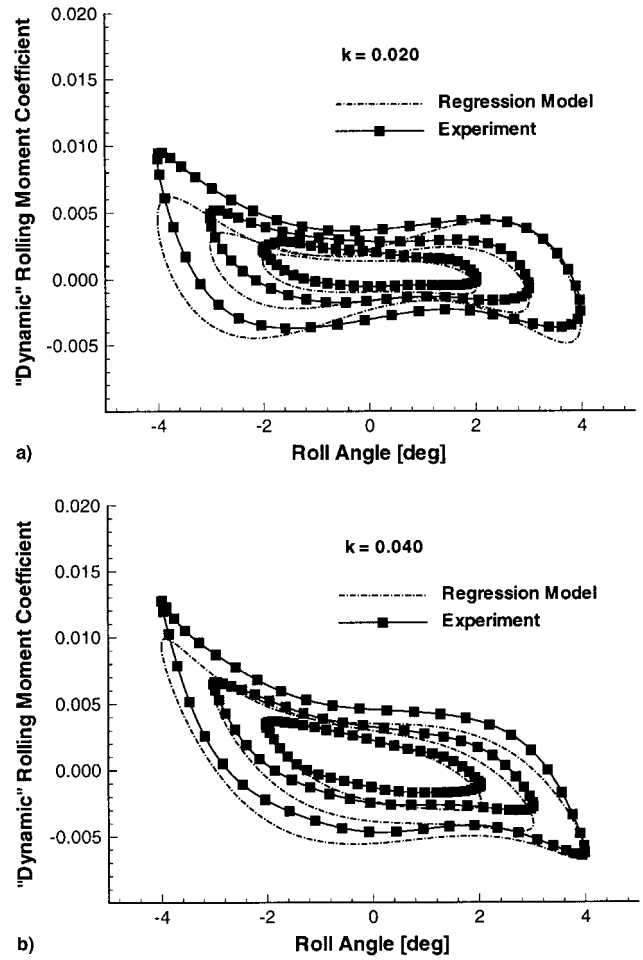

Fig. 10 $C_{l_{dyn}}$ **for harmonic oscillations centered at** $\phi = 0$ **deg for** $k =$ **a) 0.02 and b) 0.04.**

that some of the nonlinear contributions are somewhat faster, contradicting the assumption that the decaying loads are simple exponentials.

Conclusions

Experimental force and moment measurements were made for both harmonic and ramp-and-hold motions in roll. These experiments were designed to isolate critical-state effects. For the first time, evidence showing significant critical-state transients was presented. Several conclusions regarding these critical-state transients are as follows.

1) Severe time lags ($t^*_{63\%} \approx 30$) existed for motions during which a critical state was not crossed (for -4 deg $< \phi < 4$ deg). Therefore, stability derivatives are not valid for reduced frequencies, $k \geq 0.033$.

2) An independent assessment of the longest time-scales in the $|\phi| < 5$-deg range based on relationships between stability derivatives and indicial response characteristics confirmed $t^*_{63\%} \approx 30$. Also, the good agreement between independent experiments also supports the validity of nonlinear indicial response theory as applied to these data.

3) Critical-state encounters often have a severe effect on the transient rolling moment behavior.

4) The 5-deg critical state yielded the longest transient effects. A relaxation time, $t^*_{63\%} \approx 70$, was found when crossing this critical state from either above or below. Crossing the range including the 5-deg critical state, however, did not yield a noticeable history effect on the subsequent response for ϕ from 6 to 7 deg.

5) The 8-deg critical state yielded slightly smaller relaxation times $t^*_{63\%} \approx 50$ compared to the 5-deg critical state. However, including the flow history response for a crossing of the 8-deg critical state yielded a noticeable history effect on the subsequent response for ϕ from 9 to 10 deg.

6) The analysis of the 11.3-deg critical state was not conclusive because the overall change in rolling moment coefficient from the end of the ramp to its steady-state value was very small.

7) Responses to roll motions at the examined angle of attack and roll angles exhibit three distinct time scales (potential, vortical, and critical-state transients). These time scales must be accounted for to achieve accurate aerodynamic models.

Acknowledgments

This work was conducted under a Joint Research Program of the U.S. Air Force Office of Scientific Research, Wright Laboratory, the Institute for Aerospace Research, and the Canadian Department of National Defence. The support of these organizations is gratefully acknowledged.

References

[1]Jobe, C. E., Hsia, A. H., Jenkins, J. E., and Addington, G. A., "Critical States and Flow Structure on a 65-Deg Delta Wing," *Journal of Aircraft*, Vol. 33, No. 2, 1996, pp. 347–352.

[2]Jenkins, J. E., Myatt, J. H., and Hanff, E. S., "Body-Axis Rolling Motion Critical States of a 65-Degree Delta Wing," *Journal of Aircraft*, Vol. 33, No. 2, 1996, pp. 268–278.

[3]Huang, X. Z., and Hanff, E. S., "Roll Rate Induced Camber Effect on Delta Wing Leading-Edge Vortex Breakdown," AIAA Paper 95-1793, June 1995.

[4]Ericsson, L., and Hanff, E. S., "Further Analysis of High-Rate Rolling Experiments of a 65-Deg Delta Wing," *Journal of Aircraft*, Vol. 31, No. 6, 1994, pp. 1350–1357.

[5]Huang, X. Z., Hanff, E. S., Jenkins, J. E., and Addington, G., "Leading-Edge Vortex Behavior on a 65° Delta Wing Oscillating in Roll," AIAA Paper 94-3507, Aug. 1994.

[6]Huang, X. Z., and Hanff, E. S., "Prediction of Normal Force on a Delta Wing Rolling at High Incidence," AIAA Paper 93-3686, Aug. 1993.

[7]Hsia, A. H., Myatt, J. H., and Jenkins, J. E., "Nonlinear and Unsteady Aerodynamic Responses of a Rolling 65-Delta Wing," AIAA Paper 93-3682, Aug. 1993.

[8]Addington, G., and Jenkins, J., "Flow Visualization of a Rolling Delta Wing and Its Pertinence to the Nonlinear Indicial Response Model," AIAA Paper 93-3469, Aug. 1993.

[9]Huang, X. Z., and Hanff, E. S., "Prediction of Leading-Edge Vortex Breakdown on a Delta Wing Oscillating in Roll," AIAA Paper 92-2677, June 1992.

[10]Hanff, E. S., and Huang, X. Z., "Roll-Induced Cross-Loads on a Delta Wing at High Incidence," AIAA Paper 91-3223, Sept. 1991.

[11]Hanff, E. S., and Jenkins, S. B., "Large-Amplitude High-Rate Rolling Experiments on a Delta and Double Delta Wing," AIAA Paper 90-0224, Jan. 1990.

[12]Hanff, E. S., Kapoor, K., Anstey, C. R., and Prini, A., "Large-Amplitude High-Rate Roll Oscillation System for the Measurement of Non-Linear Loads," AIAA Paper 90-1426, June 1990.

[13]Jenkins, J. E., and Hanff, E. S., "Highlights of the IAR/WL Delta Wing Program," AIAA Workshop on Delta Wings: Unsteady Aerodynamics and Modeling, Atmospheric Flight Mechanics Conf., Aug. 1995.

[14]Youngren, H. H., Bouchard, E. E., and Coopersmith, R. M., "Quadrilateral Element Panel Method: User's Manual Ver. 3.2," Lockheed–California Co., Burbank, CA, 1984.

[15]Tobak, M., and Chapman, G. T., "Nonlinear Problems in Flight Dynamics Involving Aerodynamic Bifurcations," *AGARD Symposium on Unsteady Aerodynamics—Fundamentals and Applications to Aircraft Dynamics*, CP-386, AGARD, 1985, pp. 25-1–25-15.

[16]Tobak, M., Chapman, G. T., and Unal, A., "Modeling Aerodynamic Discontinuities and Onset of Chaos in Flight Dynamical Systems," *Annales des Telecommunications*, Tome 42, Nos. 5, 6, 1987, pp. 300–314; also NASA TM-89420, Dec. 1986.

[17]Jenkins, J. E., "Simplification of Nonlinear Indicial Response Models: Assessment for the Two-Dimensional Airfoil Case," *Journal of Aircraft*, Vol. 25, No. 2, 1991, pp. 131–138.